

# A Laser Flash Photolysis/Time-Resolved FTIR Emission Study of a New Channel in the Reaction of $\text{CH}_3 + \text{O}$ : Production of $\text{CO}(\nu)$

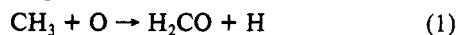
Paul W. Seakins<sup>†</sup> and Stephen R. Leone<sup>\*†</sup>

Joint Institute for Laboratory Astrophysics, National Institute of Standards and Technology and University of Colorado, and Department of Chemistry and Biochemistry, University of Colorado, Boulder, Colorado 80309-0440 (Received: November 18, 1991; In Final Form: January 27, 1992)

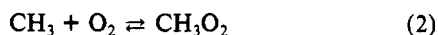
The reaction of  $\text{CH}_3$  radicals and O atoms is studied using laser flash photolysis/time-resolved Fourier transform infrared emission spectroscopy. In addition to observing formaldehyde vibrational CH emission, molecular CO vibrational emission is also detected. Experiments are performed to confirm that CO is a primary product from the title reaction. The observed CO vibrational distribution ( $\nu = 1-8$ ) can be fit with a vibrational temperature of  $12\,700 \pm 1400$  K, and the fraction of the reaction exothermicity released into CO vibration is 0.22. The branching fraction to CO is estimated to be  $0.40 \pm 0.10$ .

## Introduction

The reaction of methyl radicals with oxygen atoms (reaction 1) is of considerable importance in combustion of small hydrocarbon species.<sup>1,2</sup> Formaldehyde and hydrogen atoms are considered to be the sole products of the reaction<sup>1-3</sup>

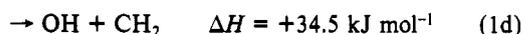
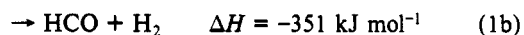


At combustion temperatures the equilibrium of the  $\text{CH}_3 + \text{O}_2$  reaction



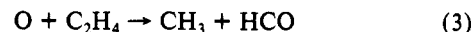
lies to the left, and under relatively lean fuel conditions reaction 1 is the major route for the removal of methyl radicals.<sup>2</sup> The kinetics of reaction 1 have been extensively studied by a number of different experimental techniques, at both low<sup>4-8</sup> and high temperatures.<sup>7,9,10</sup> A temperature-independent rate coefficient of  $(1.2 \pm 0.3) \times 10^{-10} \text{ cm}^3 \text{ molecule}^{-1} \text{ s}^{-1}$  encompasses all of the recent experimental data.

There are potentially four product channels for reaction 1, three exothermic and one endothermic:



Using a laser flash photolysis/photoionization technique, Slagle et al.<sup>7</sup> were able to monitor both the disappearance of  $\text{CH}_3$  radicals and the concurrent rise in signal corresponding to the production of formaldehyde, following the simultaneous 193-nm photolysis of  $\text{SO}_2$  to produce  $\text{O}(^3\text{P})$  and acetone to produce  $\text{CH}_3$ . No signals corresponding to either  $\text{CH}_2$  or  $\text{HCO}$  were detected. The photoionization technique is unable to observe either CO or  $\text{H}_2$  with the available light sources. Zellner et al.<sup>6</sup> measured a rate coefficient for reaction 1 by observing the production of formaldehyde with laser-induced fluorescence, following excimer laser photolysis of azomethane and  $\text{N}_2\text{O}$  to form  $\text{CH}_3$  and O atoms, respectively. Mass balance estimates in that work suggested that the predominant channel for reaction 1 is the production of formaldehyde, although no quantitative data were presented. Hoyermanns and Sievert<sup>11</sup> generated  $\text{CH}_3$  radicals by F atom abstraction from  $\text{CH}_4$  and O atoms with a microwave discharge. Mass spectrometric product analysis following electron impact ionization detected peaks at mass 29 ( $\text{HCO}$ ) and 30 ( $\text{H}_2\text{CO}$ ). A majority of the former peak was attributed to fragmentation of formaldehyde. The maximum branching fraction for reaction 1b was estimated to be 20%. No evidence was found for reaction

1d. The possibility of channel 1c does not seem to have been considered. Niki et al.<sup>12</sup> studied reaction 1 as a secondary process following the generation of methyl radicals from the reaction of oxygen atoms with ethene, reaction 3, in a discharge flow/mass spectrometry study. They estimated that 85% of reaction 1 produced formaldehyde.



Reaction 1 is assumed to proceed via a collision complex,  $\text{CH}_3\text{O}^*$ , which then dissociates to products. Quantum RRK calculations<sup>13</sup> have reproduced both the magnitude and temperature independence of the rate coefficient for reaction 1 based on this model; however, only a single exit barrier to formaldehyde production was considered.

In this paper reaction 1 has been studied using laser flash photolysis/time-resolved Fourier transform infrared (FTIR) emission spectroscopy, initially in order to examine the nascent vibrational distribution in the six infrared-active modes of the formaldehyde product. However, in addition to observing formaldehyde C-H stretch emission, strong molecular CO emission was also detected on the same time scale. A number of experiments are described here which confirm that vibrationally excited CO is produced directly in the reaction between methyl radicals and oxygen atoms. Results are presented for the vibrational distribution of CO and the branching ratio for reactions 1a-1c. A possible mechanism for the reaction and the implications of this new channel for combustion modeling are discussed.

## Experimental Section

A detailed description of the time-resolved FTIR technique has been presented elsewhere.<sup>14,15</sup> Briefly, the triggering of the pulsed

(1) Miller, J. A.; Kee, R. J.; Westbrook, C. K. *Annu. Rev. Phys. Chem.* **1990**, *41*, 345.

(2) Warnatz, J. In *Combustion Chemistry*; Gardiner, J. C., Ed.; Springer-Verlag: New York, 1983.

(3) Atkinson, R.; Baulch, D. L.; Cox, R. A.; Hampson, R. F.; Kerr, J. A.; Troe, J. *J. Phys. Chem. Ref. Data* **1989**, *18*, 881.

(4) Washida, N. *J. Chem. Phys.* **1980**, *73*, 1665.

(5) Plumb, I. C.; Ryan, K. R. *Int. J. Chem. Kinet.* **1982**, *14*, 861.

(6) Zellner, R.; Hartmann, D.; Karthaus, J.; Rhasa, P.; Weilbring, G. *J. Chem. Soc., Faraday Trans. 2* **1988**, *84*, 549.

(7) Slagle, I. R.; Sarzynski, D.; Gutman, D. *J. Phys. Chem.* **1987**, *91*, 4375.

(8) Oser, H.; Walter, D.; Stothard, N. D.; Grotheer, O.; Grotheer, H. H. *Chem. Phys. Lett.* **1991**, *181*, 521.

(9) Biordi, J. C.; Lazzara, C. P.; Papp, J. F. *Symp. (Int.) Combust., [Proc.]* **1975**, *15*, 917.

(10) Bhaskaran, K. A.; Frank, P.; Just, Th. *Symp. (Int.) Shock Tubes, [Proc.]* **1980**, *12*, 503.

(11) Hoyermanns, K.; Sievert, R. *Symp. (Int.) Combust., [Proc.]* **1979**, *17*, 517.

(12) Niki, H.; Daby, E. E.; Weinstock, B. *Symp. (Int.) Combust., [Proc.]* **1969**, *12*, 277.

(13) Dean, A. M.; Westmoreland, P. R. *Int. J. Chem. Kinet.* **1987**, *19*, 207.

<sup>†</sup>NATO/SERC Fellow.

<sup>\*</sup>Staff member, Quantum Physics Division, National Institute of Standards and Technology.

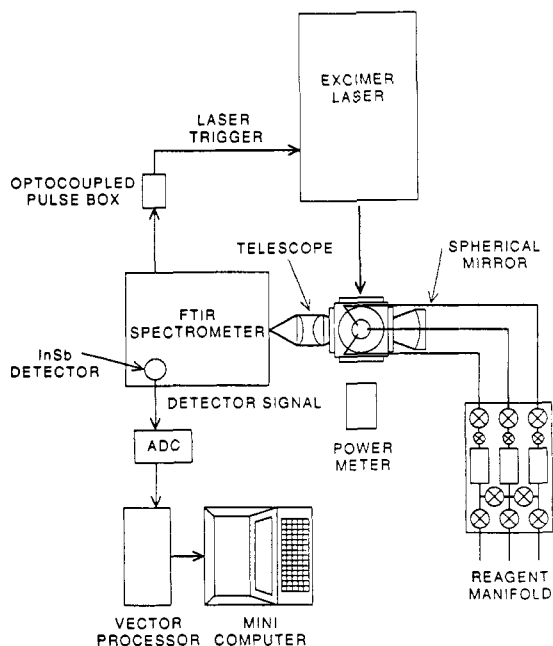


Figure 1. Schematic diagram of the experimental apparatus.

photolysis excimer laser is synchronized to the sweep of the interferometer mirror. The pulsed infrared emission from the reaction is correlated in time and with interferometer displacement by a computerized data acquisition technique. A schematic diagram of the apparatus is shown in Figure 1.

An ArF laser beam ( $\sim 80$  mJ/pulse, 1–140 Hz) is passed once through a flow cell, perpendicular to the infrared collection axis. The flow cell is a solid aluminum cube approximately 7.6 cm on a side that has been bored through on all three axes with 2.5-cm-diameter holes. Entrance and exit windows for the laser are UV quartz, while those along the interferometer axis are calcium fluoride. Reagent inlets are located on the top flange while additional buffer gas is introduced at the photolysis window to prevent the buildup of hydrocarbon films. The excimer laser beam is used to simultaneously produce both  $\text{CH}_3$  (from either acetone or methyl iodide) and O atoms from the photolysis of  $\text{SO}_2$ . Typical experimental conditions were  $\sim 1$  Pa of methyl radical precursor (methyl iodide or acetone) and 15 Pa of  $\text{SO}_2$  (1 Pa =  $7.5 \times 10^{-3}$  Torr), yielding an approximate ratio of 15:1 for the initial concentration ratios of oxygen atoms to methyl radicals. Both methyl iodide (99.9%) and acetone (99.9%) were thoroughly degassed before use. Methyl iodide was stored in a darkened bulb.  $\text{SO}_2$  (99.9%) was used directly from the lecture bottle. Buffer gases (Ar, 99.99%; He, 99.9999%;  $\text{N}_2$ , 99.999%) were also used without further purification.

Infrared emission from the reaction products is collected by two 5-cm-diameter calcium fluoride lenses forming a telescope whose output is matched to the  $f/4$  optics of the interferometer. Emission exiting the cell in the direction opposite to that of the FTIR spectrometer is back-reflected by a gold-coated spherical mirror. After passing through a suitable broad-band filter, the infrared light is detected by a 1-mm-diameter InSb element ( $D^* = 2.0 \times 10^{11}$  cm  $\text{Hz}^{1/2}$   $\text{W}^{-1}$ , 5- $\mu\text{s}$  time constant). Time-resolved total emission signals were obtained from an InSb detector (1- $\mu\text{s}$  time constant) mounted directly above the cell, viewing the infrared emission through a suitable broad-band filter. The resulting signal was recorded on a digital oscilloscope.

Time resolution in the interferogram is obtained as follows. A single-mode He:Ne laser passes through the interferometer collinearly with the infrared emission. This single-frequency laser generates a sinusoidal interference pattern on a separate detector as the moving mirror is swept (Figure 2). The zero crossings

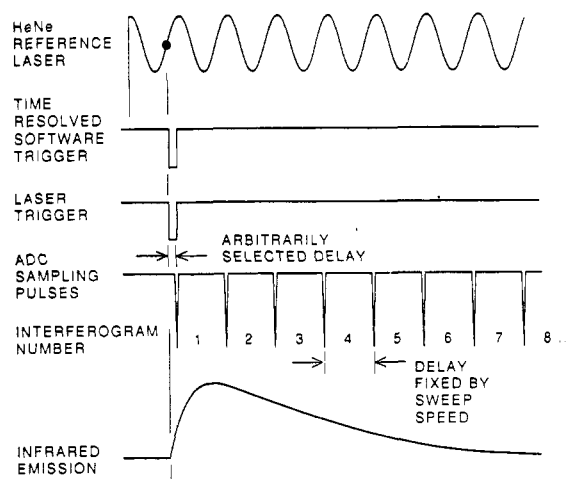


Figure 2. Schematic diagram of the interleaved sampling technique used to record time-resolved interferograms.

of the sine wave are counted by the computer with respect to the zero displacement of the interferometer and are used to keep track of the moving mirror position and to trigger the time-resolved software system that controls the data acquisition sequence. At a zero crossing the laser is triggered, and after a selectable delay (typically 5  $\mu\text{s}$  in our experiment) the infrared emission falling on the detector is digitized and the data point is assigned to the interferogram. This digitizing process is repeated at subsequent zero crossings, the time delay of which is controlled by the mirror sweep speed (typically 30–100  $\mu\text{s}$ ), until the required number of time-resolved points is obtained after a single laser pulse. A number of zero crossings are then skipped, at which time there is no laser triggering or data acquisition. The precise number of skipped fringes is determined by the mirror sweep speed and the user-selected laser triggering rate (typically 1 cm  $\text{s}^{-1}$  and  $\sim 100$  Hz in these experiments). At the start of the next sweep, the start of the laser trigger and data sampling points are incremented by one He:Ne fringe and a second set of data points is added to each interferogram. This procedure is repeated until complete interferograms are compiled at all time delays. A number of co-additions of the interferograms ( $\sim 12$ –20) were made to improve the signal to noise.

The raw interferograms are phase corrected and then Fourier transformed. Triggering in the interferometer is such that only emission after the zero-point center burst is collected. Putting a glass flat in the path of the light entering the moving mirror alters the timing so that enough signal can be collected before the center burst to allow for phase correction from the raw interferogram. Correction for the frequency-dependent transmission and reflection properties of the optics and background, as well as the detection efficiency of the detector, is obtained by ratioing the raw spectra with an instrument response function, the latter being calculated from a measured and theoretical blackbody spectrum.

## Results

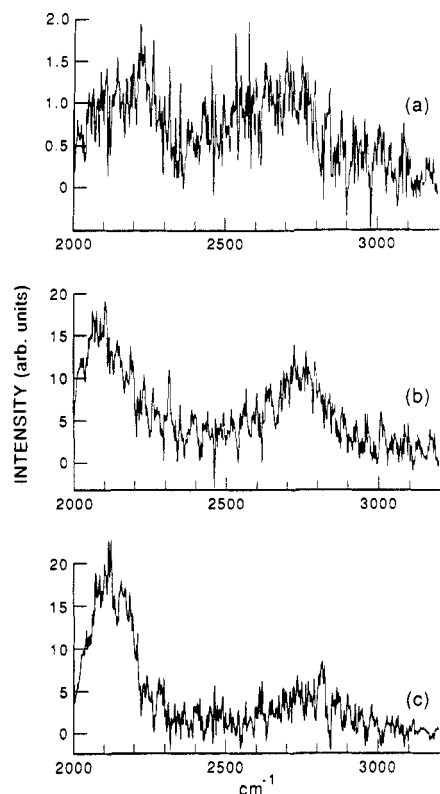
Figure 3 shows a low-resolution (5  $\text{cm}^{-1}$ ) spectrum of the region 2000–3200  $\text{cm}^{-1}$ . The peak in the region 2500–2900  $\text{cm}^{-1}$  is characteristic of formaldehyde CH stretch emission  $\nu_1$  and  $\nu_5$ . No CH emission corresponding to any other hydrocarbon product or precursor was detected. The emission to lower frequencies cannot be attributed to  $\text{H}_2\text{CO}$ , as discussed below.

Figure 4 shows part of a higher resolution (0.25  $\text{cm}^{-1}$ ) FTIR spectrum of the emission in the CO region. Each peak can be positively assigned to a CO rovibrational transition from  $\nu = 8$  to  $\nu = 1$ , providing proof that the low-frequency emission is from CO rather than any  $\text{CH}_3$  adduct.

Figure 5 shows the broad-band time-resolved, total emission traces observed through two different infrared interference filters. Figure 5a corresponds to the CH stretch emission region from formaldehyde (2500–3200  $\text{cm}^{-1}$ ) while Figure 5b,c is recorded

(14) Woodbridge, E. L.; Fletcher, T. R.; Leone, S. R. *J. Phys. Chem.* 1988, 92, 5387.

(15) Woodbridge, E. L.; Ashfold, M. N. R.; Leone, S. R. *J. Chem. Phys.* 1991, 94, 4195.



**Figure 3.** Low-resolution spectra of the emission following the photolysis of 0.8 Pa of  $\text{CH}_3\text{I}$  in the presence of 27 Pa of  $\text{SO}_2$  (133 Pa of  $\text{N}_2$  buffer): (a) 15  $\mu\text{s}$ , (b) 46  $\mu\text{s}$ , (c) 111  $\mu\text{s}$ .

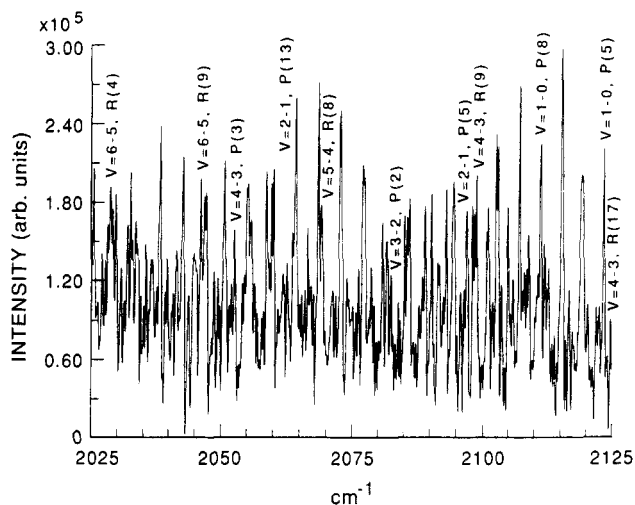


**Figure 4.** High-resolution spectra of the CO emission 60  $\mu\text{s}$  after the photolysis pulse, showing the rovibrational assignments for several peaks. The figure in parentheses refers to the rotational quantum number of the lower vibrational state (0.8 Pa of  $\text{CH}_3\text{I}$ , 15 Pa of  $\text{SO}_2$ , 133 Pa of Ar).

using a CO filter (1825–2250  $\text{cm}^{-1}$ ). Figure 5b is the signal from the photolysis of 0.8 Pa of acetone alone, while Figure 5c is the total CO emission recorded under identical conditions but with 26 Pa of  $\text{SO}_2$ . It can readily be seen that neither the CH nor CO emission signals from the reaction have the prompt rise characteristic of a photodissociation. Note that the conditions in parts a and c of Figure 5 are not identical, and therefore the rise times will not be the same. In addition, collisional deactivation of the CH emission is more rapid than for CO.

A number of checks were performed first with this time-resolved, total emission experimental configuration to confirm the identity of the reaction. All of the following experiments were carried out with the concentration of oxygen atoms in excess to that of methyl radicals ( $\sim 15:1$ ).

(1) Two different methyl radical precursors, acetone and methyl iodide, were used. Both yielded formaldehyde and CO emission.

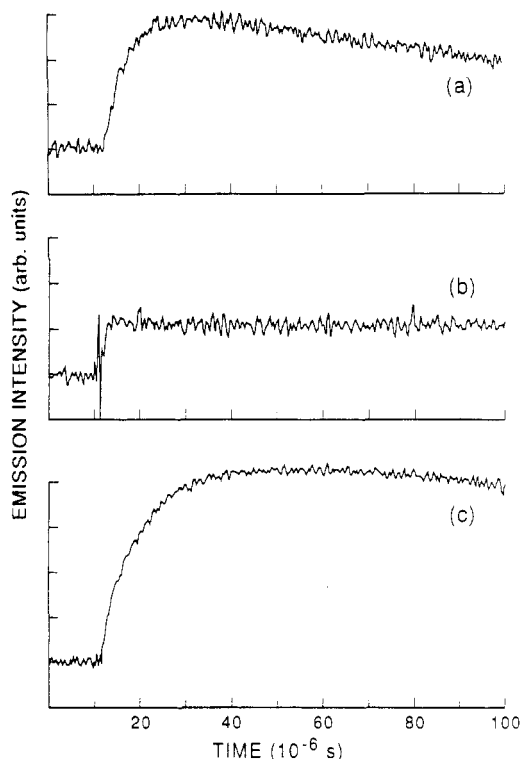
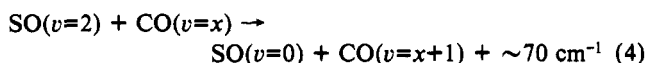


**Figure 5.** (a) Total emission observed through a broad-band interference filter (2500–3200  $\text{cm}^{-1}$ ) corresponding to  $\text{H}_2\text{CO}(v)$  emission (0.8 Pa of  $\text{CH}_3\text{I}$ , 40 Pa of  $\text{SO}_2$ , 133 Pa of  $\text{N}_2$ ). The time scale is 10  $\mu\text{s}/\text{division}$  for each trace. (b) Total emission observed through a broad-band interference filter (1850–2250  $\text{cm}^{-1}$ ) corresponding to  $\text{CO}(v)$  emission (0.8 Pa of acetone, 133 Pa of  $\text{N}_2$ ). (c) As in (b) but with 26 Pa of  $\text{SO}_2$ .

Of course, acetone photolysis itself yields vibrationally excited CO (Figure 5b);<sup>14</sup> however, its appearance is prompt and approximately a factor of 7 less than that produced by the reaction for the same concentration of acetone (Figure 5b,c).

(2) No signal ( $<1\%$ ) was observed in either of the above spectral regions with the photolysis of methyl iodide alone. Photolysis of high concentrations of  $\text{SO}_2$  alone ( $>15$  Pa) produced a small signal when observed through the CO interference filter (less than 3% of the signal observed from reaction 1 when the O: $\text{CH}_3$  ratio is 15:1). The photolysis of  $\text{SO}_2$  yields  $\text{O}(^3\text{P})$  and  $\text{SO}(^3\Sigma^-)$ . The vibrational distribution of the diatomic product is reported to be strongly inverted, peaking at  $v = 2$  ( $v = 0/1/2/3 = 0.05/0.20/0.70/0.05$ ).<sup>16</sup> No CO vibrational emission ( $<1\%$ ) was observed from the photolysis of  $\text{SO}_2$  in the presence of CO (0.1–5 Pa), showing that, as expected, there is no V-V transfer from reaction 4.



(3) Figure 6a shows the variation in peak amplitude of the  $\text{H}_2\text{CO}$  and CO signals as a function of methyl radical precursor at constant laser energy (60 mJ) and fixed  $\text{SO}_2$  pressure (26 Pa,  $\sim 200$  mTorr). As would be expected when the oxygen atoms are in excess, the signal amplitudes scale directly with methyl radical precursor concentration, showing a first-order dependence on methyl radical concentration.

(4) The concentration of oxygen atoms was varied by altering the  $\text{SO}_2$  pressure. Figure 6b shows the variation in signal amplitude in the CO region with different partial pressures of  $\text{SO}_2$ . Again, as would be expected when O atoms are in excess, there is no systematic variation in signal intensity with respect to oxygen atom concentration. Below 8 Pa of  $\text{SO}_2$  the signal starts to decrease slightly, indicating the possibility of some side reactions of  $\text{CH}_3$  when the O atoms are not in large excess. This effect is present in both spectral regions. All kinetic results and FTIR

(16) Kawasaki, M.; Sato, H. *Chem. Phys. Lett.* **1987**, *139*, 585.

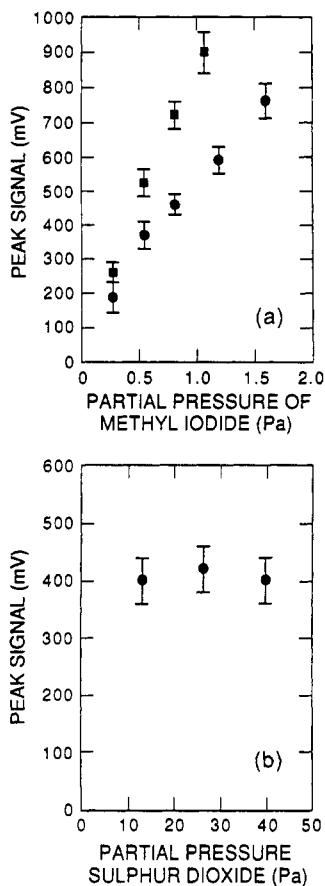
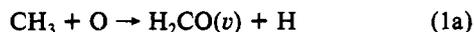


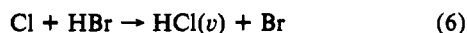
**Figure 6.** (a) Variation in peak signal intensity with CH<sub>3</sub>I partial pressure: ●, H<sub>2</sub>CO filter; ■, CO filter; constant 26 Pa of SO<sub>2</sub> and 133 Pa of Ar. (b) Variation in peak signal intensity with SO<sub>2</sub> partial pressure, observed through CO filter. Constant 0.8 Pa of CH<sub>3</sub>I and 133 Pa of Ar.

studies were performed with a partial pressure of greater than 15 Pa of SO<sub>2</sub>.

(5) An estimate of the rate coefficient for formaldehyde formation was made by fitting the C–H stretch emission to the following kinetic model



where reaction 5 represents an overall pseudo-first-order deactivation process for vibrational relaxation of excited CH stretches in formaldehyde. The O atom concentration is estimated from the photolysis cross section at 193 nm, the partial pressure of SO<sub>2</sub>, and the measured laser fluence. Figure 7 shows the resulting biexponential fit to the data, yielding a rate coefficient for H<sub>2</sub>CO production of  $(9.4 \pm 3.0) \times 10^{-11} \text{ cm}^3 \text{ molecule}^{-1} \text{ s}^{-1}$ , in reasonable agreement with the literature value  $(1.2 \pm 0.3) \times 10^{-10} \text{ cm}^3 \text{ molecule}^{-1} \text{ s}^{-1}$ . Simple biexponential fits did not match the CO signal as well, and resulting values for the rate coefficient ( $6.0 \times 10^{-11} \text{ cm}^3 \text{ molecule}^{-1} \text{ s}^{-1}$ ) were approximately 30% less than for formaldehyde formation with a significantly increased error ( $\pm 50\%$ ). A possible explanation for these discrepancies is the complex vibrational cascade and radiative lifetime kinetics from  $v = 8$  to  $v = 1$  in the product CO. For example, rate coefficients for reaction 6 measured by monitoring broad-band emission from



the vibrationally excited product HCl were shown to be 20–30% lower than measurements made by state-selective observation of the highest vibrational state of HCl ( $v = 2$ ).<sup>17</sup> The latter de-

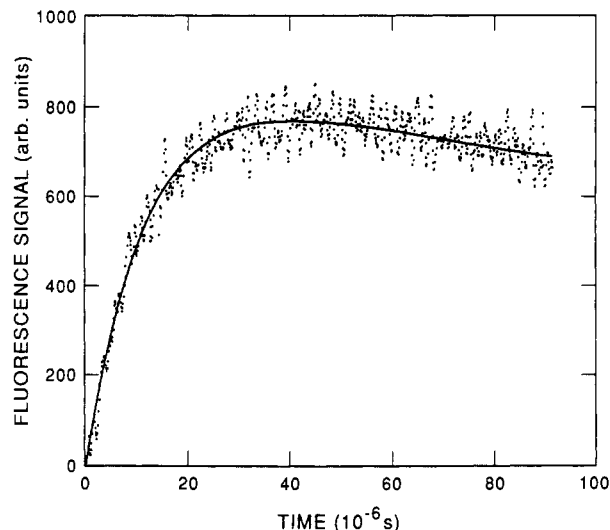


**Figure 7.** Biexponential fit to observed profile of H<sub>2</sub>CO(*v*) emission following photolysis of 2 Pa of CH<sub>3</sub>I and 40 Pa of SO<sub>2</sub> in 530 Pa of Ar.

terminations are free from cascade effects. As will be discussed below, the observed difference in rise times for the two regions of spectral observation is small compared to the difference which would occur if CO is generated from secondary reactions of formaldehyde.

(6) Vibrational excitation of methyl reactants might have some effect on the dynamics of reaction 1. UV photolysis of methyl iodide yields methyl radicals with significant vibrational excitation in the  $\nu_1$ <sup>18</sup> and  $\nu_2$  “umbrella” mode.<sup>19,20</sup> The 193-nm photolysis of acetone or acetone-*d*<sub>6</sub> has also been shown to produce methyl radicals with vibrational activation in both  $\nu_2$ <sup>21</sup> and  $\nu_3$ ,<sup>22</sup> the asymmetric CH stretch mode. In a series of experiments the argon buffer gas pressure was varied from 20 to 600 Pa (0.3 to 9 Torr) with little variation (<10%) in the magnitude of the CO or formaldehyde signal. At the highest argon pressure the lifetimes of the  $\nu_2$  (ca.  $0.5 \mu\text{s}$ <sup>19</sup>) and  $\nu_3$  (ca.  $5 \mu\text{s}$ <sup>22</sup>) vibrationally excited states are short compared to that for reaction (ca.  $30 \mu\text{s}$ ), and hence there appears to be a negligible effect from vibrational excitation of the methyl radical.

(7) Helium and nitrogen buffer gases (60–120 Pa) were used to check for the presence of hot H atoms (from minor photolysis channels) or electronically excited O atom reactions (produced from a multiphoton dissociation). Helium is an excellent moderator of translationally excited H atoms, while 60 Pa of N<sub>2</sub> would rapidly deactivate any O(<sup>1</sup>D) formed. The same amplitude of CO emission (within 10%) was observed with either buffer gas, compared to that detected with identical radical concentrations and argon buffer gas. In addition, the magnitude of the CO signal from the reaction when using an acetone precursor, compared to that produced from the photolysis of an identical partial pressure of acetone (Figure 5b,c) is large enough to rule out the possibility of minor photolysis channels as a source of the CO signal.

(8) There was no dependence (<5%) in the rise time of either signal on the laser repetition rate (1–120 Hz), suggesting that photolysis of, or reaction with, product species is not a significant factor.

Analysis of the nascent CO vibrational distribution ( $v = 1-8$ ) was obtained from the FTIR spectra. Unfortunately, there are not enough resolved rotational lines in each vibrational level to allow a measurement of the relative vibrational population for each time delay, even at  $0.25\text{-cm}^{-1}$  resolution. In order to extract

(18) Continetti, R. E.; Balko, B. A.; Lee, Y. T. *J. Chem. Phys.* **1988**, *89*, 3383.

(19) Hermann, H.; Leone, S. R. *Chem. Phys. Lett.* **1982**, *89*, 183.

(20) Sparks, R. K.; Shobotake, K.; Carlson, L. R.; Lee, Y. T. *J. Chem. Phys.* **1981**, *75*, 3838.

(21) Hall, G. E.; Vanden Bout, D.; Sears, T. J. *J. Chem. Phys.* **1991**, *94*, 4182.

(22) Donaldson, D. J.; Leone, S. R. *J. Phys. Chem.* **1987**, *91*, 3128.

(17) Dolson, D. A.; Leone, S. R. *J. Phys. Chem.* **1987**, *91*, 3543.

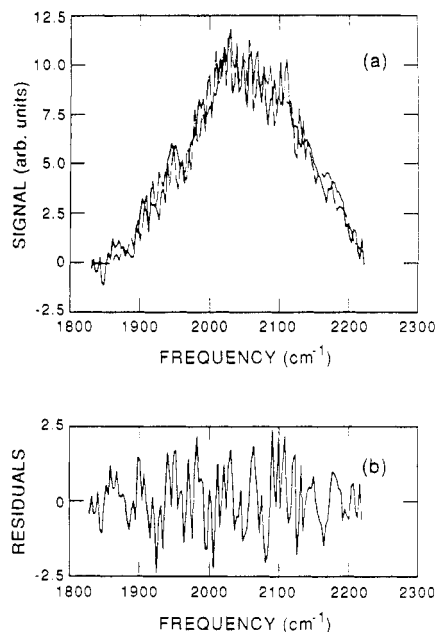


**Figure 8.** (a) Fit and (b) residuals to a low-resolution CO spectrum: (—) data; (---) fit.

**TABLE I: CO Vibrational Populations**

vibrational quantum no.	nascent rel vibrational population	rel population at 200 $\mu$ s from fit to low-resolution spectrum ( $v = 1-3$ only)	rel population at 200 $\mu$ s from peak heights ( $v = 1-3$ only)
1	$0.27 \pm 0.04$	$0.57 \pm 0.05$	$0.61 \pm 0.05$
2	$0.19 \pm 0.03$	$0.28 \pm 0.03$	$0.26 \pm 0.03$
3	$0.15 \pm 0.02$	$0.15 \pm 0.02$	$0.13 \pm 0.01$
4	$0.12 \pm 0.02$		
5	$0.08 \pm 0.01$		
6	$0.06 \pm 0.01$		
7	$0.08 \pm 0.02$		
8	$0.05 \pm 0.01$		

this information, lower ( $2.0 \text{ cm}^{-1}$ ) resolution spectra of CO were fit with Boltzmann rotational envelopes of each vibrational level. Using the known Einstein  $A$  coefficients,<sup>23</sup> the relative vibrational populations were floated using a nonlinear least-squares program until the best fit was achieved (Figure 8). Vibrational analysis was performed for each time delay, and nascent distributions were obtained by linear extrapolations. The results are shown in column 2 of Table I and correspond to a vibrational temperature of  $12\,700 \pm 1400 \text{ K}$  (Figure 9). Assuming that  $\text{CO}(v=0)$  can be estimated by extrapolation of the Boltzmann plot, then the fraction of energy released as CO vibration is 0.22. There were enough resolved lines in the first three vibrational levels at longer time delays to confirm the validity of this technique in determining relative vibrational populations. The comparison between relative vibrational populations determined by comparing peak heights and via the fitting technique is shown in columns 3 and 4 of Table I.

From the series of time-resolved low-resolution ( $5.0 \text{ cm}^{-1}$ ) FTIR spectra in Figure 3, it can be seen that there is considerable intensity in the C-H stretch region ( $2500\text{--}3000 \text{ cm}^{-1}$ ). The peak shifts with time to higher frequencies consistent with the fundamental transitions of  $\nu_1$  ( $2780 \text{ cm}^{-1}$ ) and  $\nu_5$  ( $2874 \text{ cm}^{-1}$ ), which are the symmetric and antisymmetric C-H vibrational frequencies, respectively. The C-H stretch frequencies for the precursor species (acetone or methyl iodide) occur at higher values (ca.  $3000 \text{ cm}^{-1}$ ). In addition, this spectral region can also contain a number of combination transitions including  $\nu_2 + \nu_4$  ( $2913 \text{ cm}^{-1}$ ),  $\nu_2 + \nu_6$  ( $2995 \text{ cm}^{-1}$ ),  $\nu_3 + \nu_4$  ( $2667 \text{ cm}^{-1}$ ),  $\nu_3 + \nu_6$  ( $2750 \text{ cm}^{-1}$ ), and  $2\nu_3$  ( $3000 \text{ cm}^{-1}$ ). Due to the complexity of this region, detailed resolution has not been attained, but the presence of significant

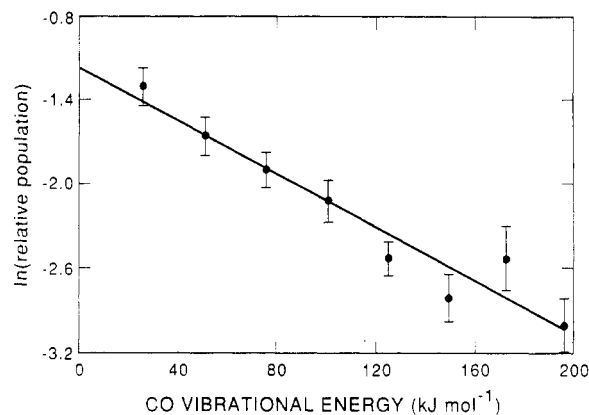


**Figure 9.** Boltzmann plot of the CO vibrational distribution produced from reaction 1c.

intensity at frequencies below that expected for the fundamental or combination frequencies of formaldehyde suggests that the formaldehyde is born with considerable vibrational excitation. The lower frequency regions of the spectra show similar trends for carbon monoxide, with the initial high vibrational excitation relaxing toward the  $v = (1 \rightarrow 0)$  fundamental transition centered at  $2150 \text{ cm}^{-1}$ .

An estimate of the branching fraction for reaction 1a was obtained by comparing the total CO emission from the photolysis of a known concentration of acetone with that produced from the reaction of oxygen atoms with the same initial acetone concentration. The methyl radical concentration is twice the CO concentration in the photolysis of acetone. The vibrational distribution of CO from acetone photolysis is well-known<sup>14,24</sup> ( $v = 0/1/2/3 = 0.75/0.18/0.06/0.01$ ) and acts as a calibration for the system. It is assumed that all the methyl radicals react via either channel 1a or 1c, yielding the same  $\text{CO}(v)$  vibrational distribution as observed with methyl iodide as a precursor. Under the experimental conditions  $\sim 99\%$  of the methyl radicals are expected to react via reaction 1.<sup>7</sup> By ratioing the  $\text{CO}(v)$  signals and correcting for the known vibrational distributions and Einstein  $A$  coefficients, a branching fraction of  $0.4 \pm 0.1$  is obtained for the production of CO. The large error bars arise from uncertainty in the nascent  $\text{CO}(v)$  vibrational distribution from  $\text{CH}_3 + \text{O}$  and the assumption that the relative population in  $v = 0$  can be determined from a linear extrapolation of the Boltzmann plot of Figure 9.

## Discussion

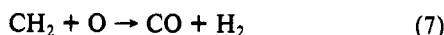
A number of checks have been performed to confirm that  $\text{CO}(v)$  is a direct product of the reaction of methyl radicals with oxygen atoms. Unambiguous assignment of CO rovibrational emission produced on the same time scale as formaldehyde emission has been confirmed. Potential complications due to vibrational excitation of methyl radicals, electronically or translationally excited atom reactions, product photolysis, and reaction with residual products have been eliminated as possible causes for the CO signal observed. The  $\text{CO}(v)$  product displays the correct kinetic orders with variation of  $[\text{CH}_3]$  and  $[\text{O}]$  atoms, when the latter is in excess. Below we enumerate a number of other considerations which verify the origin of the  $\text{CO}(v)$  emission.

Slagle et al.<sup>7</sup> performed extensive tests to confirm that  $\text{SO}_2$  and acetone are ideal precursors for the study of reaction 1. The photolysis of all the precursors at  $193 \text{ nm}$  has been well documented<sup>7,14,18,20,21,24,25</sup> and shown to yield either  $\text{O}(^3\text{P})$  or  $\text{CH}_3$  as the predominant channel. The radical  $\text{CH}_2$  is a minor secondary photolysis product from the photodissociation of acetone at  $193 \text{ nm}$ . This radical is thought<sup>25</sup> to be produced by photolysis of vibrationally excited methyl radicals. The reaction of  $\text{CH}_2$  with oxygen atoms is known to produce  $\text{CO}$ .<sup>26</sup>

(24) Trentleman, K. A.; Kable, S. H.; Moss, D. B.; Houston, P. L. *J. Chem. Phys.* **1989**, *91*, 7498.

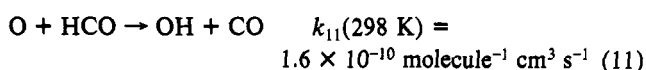
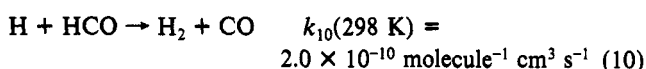
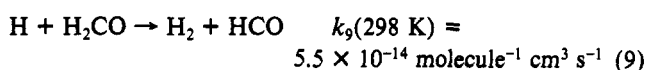
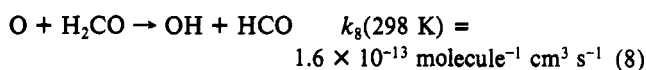
(25) Lightfoot, P. D.; Kirwan, S. P.; Pilling, M. J. *J. Phys. Chem.* **1988**, *92*, 4938.

(23) Wight, C. A.; Leone, S. R. *J. Chem. Phys.* **1983**, *78*, 4875.



There is some controversy as to the rate coefficient for reaction 7: Tsang and Hampson<sup>27</sup> recommend a value a factor of 10 smaller than that for reaction 1. However, the most recent direct determination<sup>28</sup> yielded a value comparable to that of  $k_1$ . At the maximum laser fluences used in these experiments, the initial concentration of methylene from the photolysis of acetone would be expected to be approximately 1.5% of the methyl radical concentration.<sup>25</sup> Continetti et al.<sup>18</sup> have recently studied the photolysis of methyl iodide at 193 nm by time-of-flight mass spectrometry. They determined a threshold laser fluence of 10 MW cm<sup>-2</sup> for the production of methylene. The maximum laser fluences in our experiments with CH<sub>3</sub>I are at least a factor of 2 below this value. The large magnitude and time evolution of the observed CO signal indicate that the CO(*v*) production does not come from any impurities or minor photolysis channels.

Subsequent atom abstractions from formaldehyde could also yield CO as a final product via reactions



However, the rate coefficients<sup>27</sup> for the initial hydrogen atom abstractions from formaldehyde are several orders of magnitude smaller than for reaction 1. Numerical simulations have shown that any CO production involving secondary reactions from formaldehyde would occur on time scales which are orders of magnitude longer than observed.

A CO product channel has not been observed in any of the previous studies of reaction 1. Many of the kinetic determinations have only monitored reactant decay as a function of time and made no attempt to determine branching ratios. Studies of product formation<sup>4,6,7,11</sup> have only monitored formaldehyde production, the time dependence of which does not yield any information about the branching ratio. H<sub>2</sub> and CO molecules are difficult species to detect. Their ionization potentials are very high (14.01 eV (CO), 15.43 eV (H<sub>2</sub>)), making detection by conventional photoionization mass spectrometry impossible, and obscuring signals from the decomposition of less stable reactants or products make them difficult to detect by conventional mass spectrometry. At the high electron impact energies required to monitor CO, fragmentation of formaldehyde would also yield peaks at mass 28, and fragmentation of any hydrogen-containing species could yield H<sub>2</sub>. High-temperature pyrolysis studies have extracted  $k_1$  from analysis of a complex mixture of products which would include CO and H<sub>2</sub> produced from a variety of other reactions.

Niki et al.<sup>12</sup> reported that 85% of reaction 1 produced formaldehyde. However, reaction 1 was a secondary reaction in the system, and the measured rate coefficient ( $k_1 \geq 3.0 \times 10^{-11} \text{ cm}^3 \text{ molecule}^{-1} \text{ s}^{-1}$ ) is far from the presently accepted value. In addition, CO concentrations could not be quantitatively determined, and the ratio of  $k_{10}:k_{11}$  (3:1) required to fit the experimental H<sub>2</sub> profiles is higher than the presently accepted value (~1:1).<sup>27</sup> The complexity of the system studied by Niki et al. and the new determinations of the rate coefficients required to model such a sequence of reactions coupled with the uncertainties in the determination of our own branching ratios lead us to believe that

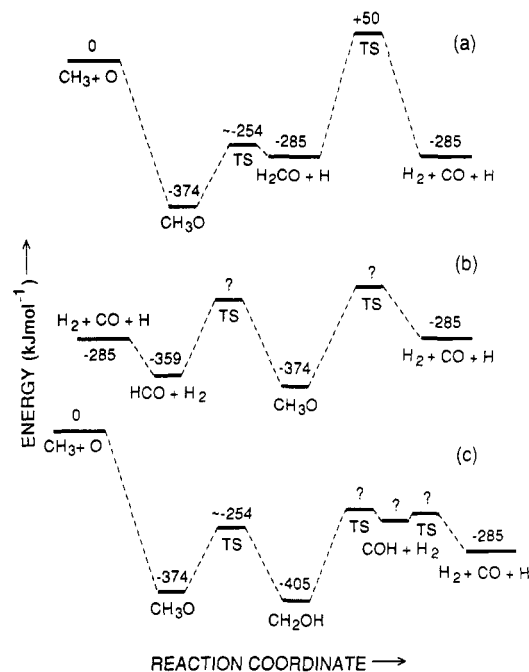


**Figure 10.** Schematic diagrams of possible potential energy surfaces for reaction 1. (a) Production of H<sub>2</sub>CO from a methoxy intermediate (note that the barrier height for production of CO lies above the entrance channel). (b) Potential routes to form CO from a methoxy intermediate. (c) Formation of the methoxy intermediate, followed by isomerization to CH<sub>2</sub>OH. COH is produced by the elimination of H<sub>2</sub>. Metastable COH decomposes to form CO + H. H<sub>2</sub>CO could be formed from CH<sub>2</sub>OH isomer by O-H bond scission (not shown).

the results of our studies are not incompatible with those of Niki et al.

Thus, we believe the previous studies were not well-suited to detect either CO or H<sub>2</sub>; in contrast, the time-resolved emission method clearly reveals the production of CO(*v*).

The CH<sub>3</sub> reaction with O atoms is presumed to proceed via the formation of a methoxy (CH<sub>3</sub>O) complex;  $\beta$  scission of an H atom from this species will yield formaldehyde. Ab initio studies have calculated the barrier height for decomposition of formaldehyde to form CO and H<sub>2</sub>.<sup>29</sup> An average of the many recent values listed in ref 29 gives a barrier height of  $353 \pm 18 \text{ kJ mol}^{-1}$  on the ground-state singlet surface. The exothermicity ( $285 \text{ kJ mol}^{-1}$ ) of reaction 1a is significantly less than this barrier, and therefore direct production of CO from the decomposition of product formaldehyde is not expected to occur. In addition, the vibrational distribution of CO produced on the singlet surface has been shown to be very different from that observed in this study.<sup>29-31</sup> Photolysis of formaldehyde, to produce H<sub>2</sub> and CO, occurs at wavelengths less than 347 nm ( $=345 \text{ kJ mol}^{-1}$ ) via the first excited singlet state. Internal conversion to the ground singlet state is followed by collisionless dissociation to molecular products. Product studies<sup>29-31</sup> have shown CO to have very little vibrational excitation following photolysis of H<sub>2</sub>CO at threshold wavelengths, with only 10% of the CO being produced in  $v = 1$  and no measurable amounts of more highly vibrationally excited products, in sharp contrast to the CO(*v*) observed from reaction 1. Thus, subsequent rapid dissociation of the formaldehyde produced in channel 1a by the same mechanism as in the photodissociation reaction cannot be the source of the CO observed in this study.

Alternatively, elimination of H<sub>2</sub> from the methoxy complex would yield HCO with  $359 \text{ kJ mol}^{-1}$  to be distributed between the two products. There have been no calculations or estimates of the barrier height for this process. However, it should be remembered that the methoxy complex is formed with considerable

(26) Shaub, W. M.; Hsu, D. S. Y.; Burks, T. L.; Lin, M. C. *Symp. (Int.) Combust., [Proc.]* **1981**, *13*, 811.

(27) Tsang, W.; Hampson, R. F. *J. Phys. Chem. Ref. Data* **1986**, *15*, 1087.

(28) Bohland, T.; Temps, F.; Wagner, H. *Gg. Ber. Bunsen-Ges. Phys. Chem.* **1984**, *88*, 1222.

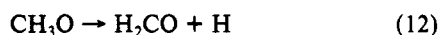
(29) Moore, C. B.; Weisshaar, J. C. *Annu. Rev. Phys. Chem.* **1983**, *34*, 525.

(30) Houston, P. L.; Moore, C. B. *J. Chem. Phys.* **1976**, *65*, 757.

(31) Cheng, C.-K.; Ho, P.; Moore, C. B.; Zughul, M. B. *J. Phys. Chem.* **1983**, *87*, 296.

excess energy which could be used to overcome significant energy barriers. The C–H bond strength in HCO is comparatively weak (ca. 60 kJ mol<sup>-1</sup>), and subsequent decomposition of HCO would yield CO. The potential surfaces for this system are illustrated schematically in Figure 10a,b.

An alternative explanation has been suggested by Wagner<sup>32</sup> (Figure 10c). Isomerization of the methoxy complex leads to the formation of the more stable isomer, CH<sub>2</sub>OH. Simple O–H bond fission now produces formaldehyde. Elimination of H<sub>2</sub> would give metastable COH, which would also rapidly decompose to form H + CO. Studies by Wagner have shown that CH will insert into H<sub>2</sub> to give CH<sub>3</sub> without any activation barrier. COH might be expected to react with H<sub>2</sub> in a similar manner (see Figure 10c). Comparisons of the activation barrier for reactions 12 and 13



indicate that isomerization of the methoxy radical may be able to compete with direct dissociation. Experimental values for  $E_{12}$ , the barrier height for reaction 12, range from approximately 110 kJ mol<sup>-1</sup> (107,<sup>33</sup> 115 kJ mol<sup>-1</sup><sup>34</sup>) to 143 kJ mol<sup>-1</sup>.<sup>35</sup> It is assumed that in these experiments the barrier height for reaction 12 is indeed being measured. An RRKM calculation of 108 kJ mol<sup>-1</sup> for  $E_{12}$  by Greenhill et al.<sup>36</sup> favors the lower energy values. There have been no experimental determinations of the barrier height for isomerization. Using thermochemical methods, Batt et al.<sup>37</sup> estimated a barrier height  $E_{13}$  of 109 kJ mol<sup>-1</sup>. A very recent ab initio calculation by Curtiss et al.<sup>38</sup> has determined  $E_{13}$  as 125 kJ mol<sup>-1</sup>. Hence, although values of  $E_{12}$  and  $E_{13}$  are widely spread, they do indicate that isomerization could rival direct dissociation, especially as the methoxy complex is formed with considerable excess energy.

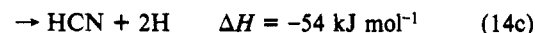
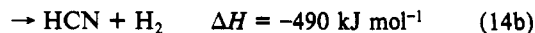
Isomerizations of addition complexes have been invoked before to describe radical–radical reactions. Wagner et al.<sup>39</sup> modeled the temperature and pressure dependence of the reaction of ethyl radicals with molecular oxygen by postulating an isomerization of the initial addition complex (C<sub>2</sub>H<sub>5</sub>O<sub>2</sub>) to CH<sub>2</sub>CH<sub>2</sub>OOH followed by decomposition to ethene and HO<sub>2</sub>. The agreement between theory and experiment is very good for this reaction scheme, indicating the validity of such complex mechanisms for radical–radical reactions.

The direct formation of CO from methoxy thermal decomposition has not been observed. There have been very few studies of this system,<sup>33–35</sup> and all have involved end product analysis of reaction mixtures where CO is expected to be present from reactions 8–11. A major difference when methoxy is formed in reaction 1 is that the methoxy intermediate is created with a large excess of energy (376 kJ mol<sup>-1</sup>). Hence, the radical–radical system may be able to surmount barriers (to both isomerizations and dissociations) and reach reaction channels that would be inaccessible in the thermal decomposition reaction.

The first electronically excited state of the methoxy radical, located 376 kJ mol<sup>-1</sup> above the ground state, is just accessible to thermal reagents. However, it is very unlikely that this intermediate would play any role in reaction 1 as it does not correlate with ground-state reagents. In addition, no experimental variation was observed in the lifetime of the excited state as the number

of vibrational quanta in the CO stretch of the excited state was increased to  $v' = 6$  (4200 cm<sup>-1</sup>, 50 kJ mol<sup>-1</sup>),<sup>40</sup> indicating that there is a barrier to product formation from the excited state of greater than 50 kJ mol<sup>-1</sup>.

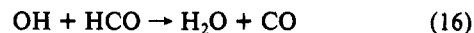
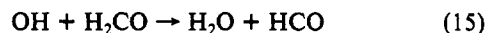
The fact that the nascent vibrational CO population can be fitted to a temperature is suggestive that it is formed from the breakup of a complex rather than a direct reaction. Indeed, it is difficult to postulate any direct mechanism that would lead to CO formation. The analogous reaction of N atoms with methyl radicals has been extensively studied by Marston et al.<sup>41–43</sup> Branching ratios for channels 14a–14c have been shown to be



0.9:0.1:0.0.<sup>43</sup> The production of HCN + H<sub>2</sub> is spin forbidden, whereas all the exothermic channels for reaction 1 are allowed. The studies of Marston et al. indicate that 1,1-eliminations from the intermediate complex are important in this type of reaction. For a pathway that was spin allowed such as reactions 1b and 1c, the branching fraction could be considerably higher than 0.1.

The effect of the CO product channel on combustion modeling is complex and dependent on the degree of combustion. Under conditions of incomplete combustion (for instance, in fuel-rich conditions), formaldehyde produced from reaction 1a may not be oxidized further. The predicted yield of formaldehyde will depend on the branching ratio of reaction 1. Given the present results, some reevaluation of the mechanisms and kinetics of the reactions involving formaldehyde production and consumption may need to be undertaken.

Under conditions of complete combustion (reactions 8–11), the equivalent OH radical reactions 15 and 16, together with the thermal decomposition reaction of HCO (reaction 17), will yield H<sub>2</sub> and CO as combustion products. Thus, eventually reactions (1a and 1c) will produce the same products:



However, steps 10, 11, and 16 are chain terminating, removing radical chain carriers from the system, and the initial hydrogen abstraction reactions 9 and 15 would tend to temporarily remove more reactive radicals (H, OH) from the combustion system. A detailed numerical investigation of a combustion system, under conditions where reaction 1 is of significance, is required to evaluate the quantitative effect of the new channel in the reaction of CH<sub>3</sub> and O.

## Summary

Infrared spectra corresponding to vibrationally excited H<sub>2</sub>CO and CO have been recorded following the photolytic production and reaction of CH<sub>3</sub> radicals and O atoms. The production of CO has not previously been observed in this reaction. A number of experiments have been performed which confirm that indeed CO is a primary product from this reaction. The branching fraction leading to CO production is approximately 40%. The nascent vibrational distribution of CO can be fit with a temperature of 12 700 K, suggesting that it is formed from the breakup of a complex rather than a direct reaction. Possible mechanisms include CO production from decomposition of a CH<sub>3</sub>O or CH<sub>2</sub>OH intermediate or even possibly from product formaldehyde. Further

(32) Wagner, A. F. Private communication.

(33) Page, M.; Lin, M. C.; He, Y.; Choudhury, T. K. *J. Phys. Chem.* **1989**, *93*, 4404.

(34) Batt, L. *Int. J. Chem. Kinet.* **1979**, *11*, 977.

(35) Zaslanko, I. S.; Mukoseev, Yu. K.; Tyurin, A. N. *Kinet. Catal.* **1988**, *29*, 244.

(36) Greenhill, P. G.; O'Grady, B. V.; Gilbert, R. G. *Aust. J. Chem.* **1986**, *39*, 1929.

(37) Batt, L.; Burrows, J. P.; Robinson, G. N. *Chem. Phys. Lett.* **1981**, *78*, 467.

(38) Curtiss, L. A.; Kock, L. D.; Pople, J. A. *J. Chem. Phys.* **1991**, *95*, 4040.

(39) Wagner, A. F.; Slagle, I. R.; Sarzynski, D.; Gutman, D. *J. Phys. Chem.* **1990**, *94*, 1853.

(40) Inoue, G.; Akimoto, H.; Okuda, M. *J. Chem. Phys.* **1980**, *72*, 1769.

(41) Stief, L. J.; Marston, G.; Nava, D. F.; Payne, W. A.; Nesbitt, F. L. *Chem. Phys. Lett.* **1988**, *147*, 570.

(42) Marston, G.; Nesbitt, F. L.; Nava, D. F.; Payne, W. A.; Stief, L. J. *J. Phys. Chem.* **1989**, *93*, 5769.

(43) Marston, G.; Nesbitt, F. L.; Stief, L. J. *J. Chem. Phys.* **1989**, *91*, 3483.

experiments and calculations on this system and on methoxy thermal decomposition at high levels of excitation would help to determine the precise mechanism for CO production.

**Acknowledgment.** We gratefully acknowledge support of this research by the Department of Energy. Additional equipment

was provided by the National Science Foundation. P.W.S. acknowledges the award of an SERC/NATO Fellowship during which time this work had been performed.

**Registry No.** CH<sub>3</sub>, 2229-07-4; CO, 630-08-0; O, 17778-80-2; SO<sub>2</sub>, 7446-09-5; CH<sub>3</sub>I, 74-88-4; acetone, 67-64-1; formaldehyde, 50-00-0.

## Investigation of Various Factors Influencing the Effect of Scavengers on the Radiation Chemistry following the High-Energy Electron Radiolysis of Water

Simon M. Pimblott

Radiation Laboratory, University of Notre Dame, Notre Dame, Indiana 46556 (Received: December 11, 1991; In Final Form: February 4, 1992)

Stochastic independent reaction times (IRT) simulations are used to model the fast reaction in spurs similar to those found following the high-energy electron radiolysis of water and aqueous solutions. The time dependence of the rate coefficient for the reaction of the hydrated electron or the hydroxyl radical with a scavenger is shown to be important in modeling scavenging reactions only when the steady-state rate is large, e.g. for the reactions  $e_{aq}^- + O_2$  or  $OH + Br^-$ . The calculations are used to test the accuracy of the commonly used Laplace relationship between the time dependence of the radicals and the molecular products resulting from the high-energy electron radiolysis of water and the scavenger concentration dependence of the observed yields following the radiolysis of scavenger solutions. Agreement between modeled yields for the scavenger systems and predictions of the Laplace transforms of the decay and the formation kinetics in the absence of scavenger is excellent once the time dependence of the scavenging rate coefficient has been incorporated in the Laplace relationship.

### 1. Introduction

The importance of stochastic processes in the period of fast reaction that follows the high-energy electron radiolysis of water has recently received a considerable amount of attention.<sup>1,2</sup> The interest has arisen from the recognition that conventional deterministic models<sup>3,4</sup> for the kinetics following electron radiolysis do not take proper account of the separate identities of the reactants.<sup>5,6</sup> This integer nature is of tremendous importance when the reactive system is made up of only a few reactants, as in the high-energy electron radiolysis of water. About 75% of the energy lost by the primary electron results in essentially isolated clusters of reactants which are known as spurs and which contain from 1 to 6 ionization or excitation events.<sup>7,8</sup> Two alternative stochastic techniques have been developed to model spur kinetics. The most popular approach involves the Monte Carlo simulation of the kinetics by modeling the encounter times of the reactants.<sup>9-13</sup> The second method requires the formulation and solution of a

master equation describing the time-dependent probability that a spur has a certain makeup.<sup>2,11</sup>

A number of different Monte Carlo simulation techniques have been developed.<sup>2</sup> For the most part these methods follow the trajectories of the diffusing reactants, and then the reaction is modeled by encounter.<sup>10,11</sup> This type of approach is known as random flights simulation. In a series of papers,<sup>5,6,14</sup> an alternate and very efficient Monte Carlo simulation method, the independent reaction times (IRT) model, has been developed which relies upon the independent pairs approximation of the Smoluchowski-Noyes treatment of diffusion-controlled kinetics.<sup>15</sup> This approximate simulation model has been thoroughly tested by comparison of its predictions with those of random flights Monte Carlo simulation. The agreement between the results of the two methods under conditions appropriate for high-permittivity solvents such as water is excellent, although some small errors are found for low-permittivity solvents.<sup>16</sup> The approximate IRT model involves only a small fraction of the computational cost of the random flights method.

One of the most frequently used experimental techniques in the radiation chemistry of water involves the study of the effects of an added solute, known as a scavenger, upon the reactions that follow the radiolysis of the liquid.<sup>17,18</sup> This type of experiment provides direct information about the yields of the transients created by the energy transfer from the radiation particle to water. Frequently, the experiments are also used to infer data about the decay kinetics of the reactive species<sup>19-22</sup> and about the formation

(1) Freeman, G. R. *Kinetics of Nonhomogeneous Processes. A Practical Introduction for Chemists, Biologists, Physicists and Material Scientists*; Wiley-Interscience: New York, 1987.

(2) Green, N. J. B.; Pilling, M. J.; Pimblott, S. M. *Radiat. Phys. Chem.* **1989**, *32*, 99.

(3) Schwarz, H. A. *J. Phys. Chem.* **1969**, *73*, 1928.

(4) Burns, W. G.; Sims, H. E.; Goodall, J. A. B. *Radiat. Phys. Chem.* **1984**, *23*, 143.

(5) Clifford, P.; Green, N. J. B.; Pilling, M. J. *J. Phys. Chem.* **1982**, *86*, 1318.

(6) Clifford, P.; Green, N. J. B.; Oldfield, M. J.; Pilling, M. J.; Pimblott, S. M. *J. Chem. Soc., Faraday Trans. 1* **1986**, *82*, 2673.

(7) Pimblott, S. M.; LaVerne, J. A.; Mozumder, A.; Green, N. J. B. *J. Phys. Chem.* **1990**, *94*, 488.

(8) Pimblott, S. M.; Mozumder, A. *J. Phys. Chem.* **1991**, *95*, 7291.

(9) Zaider, M.; Brenner, D. J. *Radiat. Res.* **1984**, *100*, 245.

(10) Turner, J. E.; Hamm, R. N.; Wright, H. A.; Magee, J. L.; Chatterjee, A.; Hamm, R. N.; Bolch, W. E. *Radiat. Phys. Chem.* **1988**, *32*, 503.

(11) Clifford, P.; Green, N. J. B.; Pilling, M. J.; Pimblott, S. M.; Burns, W. G. *Radiat. Phys. Chem.* **1987**, *30*, 125.

(12) Green, N. J. B.; Pilling, M. J.; Pimblott, S. M.; Clifford, P. *J. Phys. Chem.* **1990**, *94*, 251.

(13) Pimblott, S. M.; Pilling, M. J.; Green, N. J. B. *Radiat. Phys. Chem.* **1991**, *37*, 377.

(14) Clifford, P.; Green, N. J. B.; Pilling, M. J.; Pimblott, S. M. *J. Phys. Chem.* **1987**, *91*, 4417.

(15) Noyes, R. M. *Prog. React. Kinet.* **1961**, *1*, 129.

(16) Green, N. J. B.; Pilling, M. J.; Pimblott, S. M.; Clifford, P. *J. Phys. Chem.* **1989**, *93*, 8025.

(17) Buxton, G. V. In *Radiation Chemistry. Principles and Applications*; Farhataziz, Rodgers, M. A. J., Eds.; VCH Publishers: Cambridge, U.K., 1987.

(18) Spinks, J. W. T.; Woods, R. J. *An Introduction to Radiation Chemistry*; Wiley-Interscience: New York, 1990.

(19) Balkas, T. I.; Fendler, J. H.; Schuler, R. H. *J. Phys. Chem.* **1970**, *74*, 4497.